LU NV 21-05
Dec 2021

Calculation of neutron scattering libraries for liquid ortho-deuterium and hydrogen deuteride

Alexander Huusko

Division of Nuclear Physics, Lund University

Master thesis supervised by Douglas Di Julio, José Ignacio Márquez Damián, and Oxana Smirnova

LUND
UNIVERSITY

Abstract

The European Spallation Source (ESS) has launched a project called HighNESS, with the task of investigating the potential of adding a second moderator system to the facility, with ortho-deuterium (o-D2) being the main material of interest. Another moderator material which could be of interest is hydrogen deuteride (HD). The purpose of this second moderator system would be to provide a high intensity source of neutrons, compared to the high brightness of the first moderator system, as well as providing a colder neutron spectrum.

In order to accurately simulate the low-energy neutron production from moderators, the thermal scattering law (TSL) of the materials in question is needed, typically in the form of scattering libraries. Previous scattering libraries for ortho-deuterium were created based on input derived from experimental data and early theoretical models, and no scattering library exists for hydrogen deuteride. This work used a type of quantum molecular dynamics (QMD), namely ring polymer molecular dynamics (RPMD) to obtain inputs for the NJOY software wherein the scattering libraries and the cross-section were calculated for ortho-deuterium and hydrogen deuteride. Since NJOY was not developed for heterogeneous molecules such as hydrogen deuteride, it had to be extended to include models for such molecules. The quantities from the molecular dynamics simulations and the cross section of both materials were benchmarked against experimental data and simulated data from other research groups. Possible improvements and continuations beyond this work are also discussed and presented in this report.

Acknowledgements

I would like to thank Dr. Douglas Di Julio and Dr. José Ignacio Márquez Damián for their supervision and support throughout the process of this thesis.

I would also like to thank my university supervisor Dr. Oxana Smirnova for her support and giving me a place to work from when it was most needed.

I would like to express my gratitude to the European Spallation Source for the possibility to do this work with them, as well as the generous stipend provided for this work.

Last but not least, I want to express the deepest of gratitude to my family, especially my father, mother, and grandmother, for their amazing support. This thesis would not have been possible were it not for them going above and beyond to support me.

Contents

1 Introduction

1.1 The European Spallation Source, ESS

The European Spallation Source (ESS) is an international research laboratory which is currently under construction in Lund, Sweden [1]. Once completed, the ESS will provide the brightest pulsed neutron source in the world for neutron scattering studies, which will be equipped with a compact para-hydrogen moderator that is designed to generate a high-brightness source of neutrons [2]. The neutron source presented at ESS will serve a wide range of research fields using neutron scattering experiments [3]. A long standing limiting factor of neutron scattering is the intensity of neutrons, due to the low portion of produced neutrons which reach the experiment stations. This is due in part to the neutral charge of the neutron, which makes it challenging to direct the neutrons to the experimental stations. For this reason, optimization of the moderator system and beam guides are critical to the performance of the facility. It is for this purpose that ESS has employed the previously mentioned compact para-hydrogen moderator, in order to maximize the number of available neutrons for experiments which can be performed at ESS.

1.2 Future cold moderator upgrade

While the high brightness beam, obtained with the current para-hydrogen moderator employed at ESS, will satisfy a wide range of experiments, there are other fields which would benefit greatly from adding an additional moderator with the purpose of providing a higher total intensity of neutrons with emphasis on the generation of cold and very cold neutrons. A material which is currently under consideration for such an upgrade is ortho-deuterium, which has been estimated in early studies to increase the total intensity of neutrons 3-4 times the amount of the primary moderator [4], while also providing a colder neutron spectrum. Having such a high intensity neutron source would be of great interest for instruments which employ the neutron spin-echo (NSE) technique, small angle neutron scattering (SANS), and neutron imaging [5]. Furthermore, it could be used for fundamental physics experiments such as searches for neutron-antineutron oscillations, a fifth force, and more [5]. For the above mentioned reasons, a project called HighNESS [5] was recently launched to study such a high-intensity neutron source at the ESS. Another material of interest would be hydrogen deuteride, as it can either show up as a contaminant when using a moderator that contains both H_2 and D_2, or as a moderator on its own. The scattering data of a material is typically gathered in a thermal scattering library, and since no thermal scattering library exists for hydrogen deuteride, it is of interest to create one in order to investigate the moderator properties of hydrogen deuteride.

1.3 Thermal Scattering Law

The neutron cross section can be calculated using the thermal scattering law (TSL), $S(\alpha, \beta)$, where α is the dimensionless momentum transfer and β is the dimensionless energy transfer. The neutron cross section is typically stored in scattering libraries as tabulated values of $S(\alpha, \beta)$ for a range of α and β. Over the past 60 years, a number of computer codes have been developed to calculate the thermal scattering law, with the primary one being the LEAPR module in the NJOY code [6]. In order to account for the low energy coherent inelastic scattering in liquid hydrogen, a modification of the LEAPR module has been developed by Márquez Damián et al. based on the work by Granada and Gillete [7][8][9]. This modification is freely available online and referred to as NJOY-H2D2 [10].

For the purpose of this thesis, one can divide the modelling of neutron scattering into roughly two parts: the high-energy range, above a few eV, and the low-energy range, below a few eV. High-energy neutron scattering is not dependent on the chemical structure of the scattering material. However, for low-energy scattering, these structures become more significant and have to be accounted for to produce accurate results. Therefore it is important to obtain knowledge of the structure and dynamics of the scattering material on a molecular level. The early stages of the thermal scattering law relied on a series of approximations in order to account for these effects. With recent advancements in simulation techniques, such as molecular dynamics, and the increased computing power of modern computers, it has become possible to study the molecular effects in greater detail [11]. As such, new methods to calculate the thermal scattering law have been developed using data obtained from molecular simulations. One of these methods uses classical molecular dynamics to simulate the scattering molecules and calculates atomic correlation functions which are then used as an input, for the NJOY program, in order to compute the thermal scattering law [12]. While this method can be applied to water, it does not account for all the

dynamics in quantum liquids such as the molecular hydrogens. A couple of research groups have shown that by using quantum molecular dynamics, it is possible to successfully compute the atomic correlations for liquid hydrogen [13][14]. These methods have only been used so far to generate neutron scattering libraries for liquid hydrogen [15][16], but not for deuterium and hydrogen-deuteride.

1.4 Objectives

A new scattering library for liquid hydrogen was created with the path-integral molecular techniques in a previous study [15]. The aim of this work is to build upon the previous work and extend the methods to new materials. Previous scattering libraries for ortho-deuterium were created based on input derived from experimental data and early theoretical models [6][10]. This work intends to generate a new scattering library for ortho-deuterium, accounting for quantum mechanical effects through path integral molecular dynamics simulations, as well as generating a temperature dependent static structure factor of the molecular dynamics system. Furthermore, the goal of the project was to generate a scattering kernel for hydrogen deuteride using the same molecular dynamics simulations and by combining existing models in the literature, which to our knowledge has not been done before.

2 Thermal neutron scattering

The neutrons produced by spallation targets can have energies above the MeV range. These high-energy neutrons have too short of a wavelength to be used in neutron scattering experiments, and as such have to be slowed down before they become useful. The processes by which these high-energy neutrons lose their energy can be described by the simple well-established theory of elastic and inelastic collisions in the center of mass frame [17]. Once the neutrons have slowed down to thermal energies, below a few eV, the neutron energies become comparable to the kinetic energies of the scattering nuclei. Since the thermal neutron wavelength is comparable to interatomic distances, one has to take into consideration any effects arising from molecular and crystal structures of the scattering nuclei. Such effects include potential interference due to the de Broglie wavelength of the neutron being comparable to intramolecular distances along with recoil of the molecular structures.

Thermal scattering consists of elastic and inelastic scattering which is in turn divided into coherent and incoherent scattering. Inelastic scattering consists of scattering events in which the kinetic energy of the incident particle changes in the lab frame. Elastic scattering, in the lab frame, on the other hand describes the scattering events in which the kinetic energy of the incident particle is conserved. Thermal neutrons do not have the energy required to excite individual atoms. However, the vibrational and rotational states of the molecular structure as well as the vibrational states of crystal structures, can be low enough such that a thermal neutron may cause a transition between these states. Furthermore, for neutron scattering in a liquid and a gas, excitation may also occur in the form of recoil of the scattering nuclei, commonly referred to as translational excitation. For liquids and gases, it has been shown that, due to translational excitation, no thermal elastic scattering will occur [18] and will thus not be considered in this report.

2.1 Thermal scattering law

The double differential cross section, $\frac{\delta^2\sigma}{\delta E'\delta\mu}$, with the final state energy, E', and cosine of the scattering angle, μ, can be obtained using the thermal scattering law (TSL), $S(\alpha,\beta)$, from the following equation,

$$\frac{\delta^2\sigma}{\delta E'\delta\mu} = \frac{\sigma_b}{2k_bT}\sqrt{\frac{E'}{E}}S(\alpha,\beta), \tag{2.1}$$

where σ_b is the bound scattering cross section, k_b is Boltzmann's constant, T is the temperature, E is the incident neutron energy, E' is the outgoing neutron energy, α is the dimensionless momentum transfer, and β is the dimensionless energy transfer. α and β can be described as the following,

$$\alpha = \frac{E' + E - 2\sqrt{EE'}\mu}{m/m_n k_bT}; \qquad \beta = \frac{E' - E}{k_bT}, \tag{2.2}$$

where m is the mass of the scattering atom, and m_n is is the mass of the neutron. Another way of expressing the thermal scattering law is as a change in wavenumber, Q, and the energy transfer, $\hbar\omega$,

where $\hbar$ is the reduced Planck's constant, and

$$\omega = \frac{E' - E}{\hbar}, \tag{2.3}$$

and

$$Q = \left| \frac{\vec{k}' - \vec{k}}{\hbar} \right|, \tag{2.4}$$

where $\vec{k}'$ is the final state wavevector, and $\vec{k}$ is the initial state wavevector. The two forms of the TSL mentioned above can be related by the following,

$$S(\alpha, \beta) = \frac{k_b T}{\hbar} S(Q, \omega). \tag{2.5}$$

In a similar fashion, the dimensionless quantities α and β can be related to Q and ω as the following,

$$\alpha = \frac{\hbar^2 Q^2}{2 m k_b T}, \qquad \beta = \frac{\hbar \omega}{k_b T}. \tag{2.6}$$

2.2 Neutron scattering for Molecular Hydrogens

The nucleus of the hydrogen atom consists of a single proton, with a nuclear spin $s = \frac{1}{2}$, whereas the deuterium nucleus consists of a proton and a neutron, giving it a nuclear spin of $s = 1$. With these two isotopes, one can form three diatomic molecules: H_2, D_2, and HD. The H_2 and D_2 molecules form states with total spin $S = 0, 1$ for H_2, and total spin $S = 0, 2$ for D_2. If the spins are anti-parallel, $S = 0$, the state is given the prefix para- to the molecule, for example para-hydrogen. If the spins are parallel, in which the spins are added up, it gives the prefix ortho- to the molecule, for example ortho-deuterium. For the heterogeneous case of hydrogen deuteride (HD), the spin is uncorrelated and does not align as the homogeneous D_2 and H_2 do. In this report, we will focus on the ortho-deuterium and the hydrogen deuteride molecules. In the case of ortho-deuterium, the spin correlation has to be accounted for when evaluating the total double differential cross section, which is done using the Young and Koppel model [19]. Guarini et al. [20] has provided explicit formulas for the double differential cross section for molecular hydrogens, which are expressed in terms of the self and distinct components and based on the Young-Koppel model. In this work, it is assumed that the molecules are rigid rotors, and the formula for the double differential cross-section can be written as

$$\frac{\delta^2 \sigma}{\delta E' \delta \mu} = \sqrt{\frac{E}{E'}} \left(u(Q) S_{d,c.m}(Q, \omega) + \sum_{J_0, J_1} F(Q, J_0, J_1) S_{s,c.m}(Q, \omega - \omega_{J_0 J_1}) \right) \tag{2.7}$$

where $S_{d,c.m}(Q, \omega)$ is the distinct scattering function in the molecule's center of mass frame, $S_{s,c.m}(Q, \omega)$ is the self scattering function in the molecule's center of mass frame, and $u(Q)$ and $F(Q, J_0, J_1)$ are weight functions including the bound scattering cross section, σ_b. See Equations 2.8, 2.9, 2.19, and 2.22 for more detail. The bound scattering cross section is given by

$$\sigma_b = \sigma_c + \sigma_i = 4\pi \left(a_c^2 + a_i^2 \right) \tag{2.8}$$

where σ_c is the bound coherent scattering cross section, σ_i is the bound incoherent scattering cross section, a_c is the coherent scattering length, and a_i is the incoherent scattering length. For H_2 and D_2 $u(Q)$ is

$$u(Q) = 4 a_c^2 j_0^2 (Q R^{eq}) \tag{2.9}$$

where j_0 is the spherical Bessel function of the zeroth order, and R^{eq} is the equilibrium internuclear distance.

$S_{d,c.m}(Q, \omega)$ is difficult to obtain since current quantum simulation methods are unable to provide reliable estimates for the total dynamic structure factor, along with the fact that there is no analytical model for $S_{c.m}(Q, \omega)$ for liquids other than specific cases [13]. However, $S_{d,c.m}(Q, \omega)$ can be obtained explicitly by using the Sköld approximation [21], which uses the static structure factor, $S(Q)$, and $S_{s,c.m}(Q, \omega)$ to approximate $S_{c.m}(Q, \omega)$. The Sköld approximation, as shown in Equation 2.10, has been shown to accurately reproduce the total cross section for both H_2 and D_2 [22][13]. which uses a modification of

the self part of the scattering function, along with the static structure factor $S(Q)$, in order to model the thermal scattering law.

$$S_{c.m}(Q,\omega) = S(Q)S_{s,c.m}\left(\frac{Q}{\sqrt{S(Q)}},\omega\right) \tag{2.10}$$

Using the Sköld approximation shown above, one can rewrite the distinct part of the scattering function in terms of the self part, see Equation 2.11.

$$S_{d,c.m} = S(Q)S_{s,c.m}(\frac{Q}{\sqrt{S(Q)}},\omega) - S_{s,c.m}(Q,\omega) \tag{2.11}$$

The static structure factor, used in the approximation above, can be obtained either by experimental data as well as through molecular dynamics calculations. Details on calculating the static structure factor through molecular dynamics are given in Chapter 3.

2.3 Dynamic structure factor

In NJOY, the dynamic structure factor is decomposed into several different components. This includes the solid (phonon), diffusion, and vibrational components. The translational motion is described as the convolution of the solid-like and diffusion components and is given by

$$S_{t,c.m}(Q,\omega) = S_{solid,c.m}(Q,\omega) \circledast S_{diff,c.m}(Q,\omega). \tag{2.12}$$

The total dynamic structure factor, to be used in Equation 2.7, is the convolution of each component given as

$$S_{c.m}(Q,\omega) = S_{solid,c.m}(Q,\omega) \circledast S_{diff,c.m}(Q,\omega) \circledast S_{vib,c.m}(Q,\omega) \tag{2.13}$$

2.3.1 Solid component

The solid component of the dynamic structure factor is calculated using the phonon distribution of the system, also referred to as $f_{solid}(\omega)$, which in this work is obtained through path integral molecular dynamics simulations, see Chapter 3.6 for more details. The phonon distribution is used in the Gaussian approximation [23][24], which is given by

$$I(Q,t) = e^{-\gamma(t)Q^2}, \tag{2.14}$$

where $I(Q,t)$ is the intermediate scattering function, and $\gamma(t)$ is the width function given by

$$\gamma(t) = \frac{\hbar}{m}\int_0^\infty d\omega \frac{f_{solid}(\omega)}{\omega}\left[\coth\left(\frac{\hbar\omega}{2k_BT}\right)(1-\cos\omega t) - i\sin\omega t\right]. \tag{2.15}$$

The dynamic structure factor for the solid component can then by calculated by

$$S_{solid,c.m}(Q,\omega) = \frac{1}{2\pi}\int_0^\infty dt e^{-i\omega t} I(Q,t). \tag{2.16}$$

2.3.2 Diffusion component

The diffusion component, as shown in Equation 2.17, is calculated in the LEAPR module of NJOY using the Egelstaff-Schofield model [25].

$$S_{diff,c.m}(Q,\omega) = \frac{\hbar}{k_BT}\frac{DQ^2}{\pi}e^{\frac{MD^2Q^2}{w_tk_BT} - \frac{\hbar\omega}{2k_BT}} \times \frac{\sqrt{c^2+\frac{1}{4}}}{\sqrt{\omega^2+(DQ^2)^2}} K_1\left(\frac{\hbar}{k_BT}\sqrt{c^2+\frac{1}{4}}\sqrt{\omega^2+(DQ^2)^2}\right) \tag{2.17}$$

where D is the diffusion constant, w_t is the weight of the diffusion component, and $K_1(x)$ is the modified Bessel function of the second kind.

2.3.3 Vibrational component

In order to account for the intramolecular vibrations, a discrete harmonic oscillator is employed in NJOY. The energy of an harmonic oscillator is given as,

$$E_n = \left(n + \frac{1}{2}\right)\hbar\omega_v = \left(n + \frac{1}{2}\right)E_v, \tag{2.18}$$

where E_n is the energy of level n, n is the vibrational quantum number, ω_v is the angular frequency of the oscillator, and E_v is the vibrational energy constant. We find that for ortho-deuterium $E_v = 0.386$ eV [26], and for hydrogen deuteride $E_v = 0.446$ eV [27], which are the amounts of energy needed in order for a vibrational transition to occur for the two molecules. While the average molecular energies at low temperatures are far lower than the amounts required for excitation, if an incident neutron has high enough energy it can cause transitions between the vibrational states and is thus important to include this component in our model. The weight of the vibrational movement was chosen according to the Sachs-Teller mass [28], which is discussed in more detail by Granada and Gillette [8].

2.4 Rotational models

2.4.1 Ortho-deuterium

As mentioned in Chapter 2.2, ortho-deuterium has a spin correlation which is accounted for by using the Young and Koppel model [19]. The rotational component is given by Guarini [29] and implemented in NJOY [6]. The $F(Q, J_0, J_1)$ term in Equation 2.7 is given by

$$F(Q, J_0, J_1) = s_{(J_0 J_1)} P_{J_0}(2J_1 + 1)\sum_l j_l^2(QR^{eq})(C_{000}^{J_1 J_0 l})^2, \tag{2.19}$$

where $s_{(J_0 J_1)}$ contains spin correlation information, P_J is the statistical weight factor, j_l is the spherical Bessel function of order l, R^{eq} is the equilibrium internuclear distance, and $C_{000}^{J_1 J_0 l}$ is a Clebsch-Gordan coefficient. For ortho-deuterium, J_0 sums over the odds numbers, which means that $s_{(J_0 J_1)}$ will only have two cases, when J_1 is odd, $s_{(J_0 J_1)} = a_c^2 + \frac{5a_i^2}{8}$, and even, $s_{(J_0 J_1)} = \frac{3a_i^2}{8}$. The statistical weight is given by

$$P_J = \frac{(2J+1)exp(-E_J/k_B T)}{\sum_J (2J+1)exp(-E_J/k_B T)} \tag{2.20}$$

where E_J is the rotational energy described in Equation 2.21.

$$E_J = BJ(J+1) \tag{2.21}$$

where B is the rotational constant.

2.4.2 Hydrogen deuteride

In the case of hydrogen deuteride, there are two atoms with different masses which means that a different model is required. The model by Lurie describes rigid rotor molecules whose atoms have different masses [30]. However, this notation does not include the distinct part of the TSL, see Equation 2.7, and so this model will only include the self part contributions. There has been recent work done by Guarini [20] which includes hydrogen deuteride with the distinct part of the dynamic structure factor included in the model. This work here follows the model of Lurie without the distinct part and uses the notation of Guarini for consistency. The rotational component for hydrogen deuteride can be separated into two parts: the self term, $F_s(Q, J_0, J_1)$, and the overlap term, $F_o(Q, J_0, J_1)$, and is given by

$$F(Q, J_0, J_1) = F_s(Q, J_0, J_1) + F_o(Q, J_0, J_1). \tag{2.22}$$

The self term describes the direct contributions of the two atoms, while the overlap term describes the contribution caused by the interference of different atoms. The self term is given by

$$F_s(Q, J_0, J_1) = P_{J_0}(2J_1 + 1)\sum_l \left[(a_{cX}^2 + a_{iX}^2)j_l^2(QR_X^{eq}) + (a_{cY}^2 + a_{iY}^2)j_l^2(QR_Y^{eq})\right](C_{000}^{J_1 J_0 l})^2 \tag{2.23}$$

where the subindices X and Y denote the two different atoms in the molecule. The overlap term is given by

$$F_o(Q, J_0, J_1) = P_{J_0}(2J_1 + 1)2a_{cX}a_{cY}\sum_l (-1)^l j_l(QR_X^{eq})j_l(QR_Y^{eq})(C_{000}^{J_1 J_0 l})^2 \tag{2.24}$$

The model proposed by Lurie is based on a free-gas model for the translational motion. In this work, we have followed the approach previously done for H_2 and D_2, where the translational component is the convolution of the solid and diffusive motion. Since NJOY was not developed for heterogeneous molecules such as hydrogen deuteride, the above mentioned model for HD had to be implemented in a new branch of the NJOY-H2D2 code [10].

3 Path-Integral Molecular Dynamics

Molecular dynamics is a method used to model materials and obtain information about their structure and dynamics on an atomic and molecular level. In order to start a molecular dynamics simulation, one sets up an initial configuration of atoms, each with an individual initial position and velocity. Furthermore, one has to define the potential field by which the atoms interact with each other. Once the initial settings have been defined, the sample runs over a series of time steps, in which the movement of each atom is determined by calculating the forces upon the atoms and solving Newton's equations of motion.

When deciding the method of modelling liquid hydrogens, it is beneficial to go for a method that incorporates quantum effects of the constituants as this has been shown to yield better agreement with experimental data [31][32]. One such method is path-integral molecular dynamics (PIMD) in which the particle moves from an initial state to a final state with an unobserved path. The formalism of PIMD is based on the Feynman path integral method and is included in molecular dynamics simulations to account for quantum effects [33]. The probability of finding the particle in the final state is calculated by integrating over all the potential paths originating from the initial state. There are two variants of PIMD which are commonly used. These include centroid molecular dynamics (CMD) [34] and ring polymer molecular dynamics (RPMD) [35]. These methods replace atoms with a number of beads which are connected through springs. RPMD was chosen for this work as an implementation of it has been made available in the open source code i-Pi [36] while resulting in nearly as good results as CMD when it comes to the quantities relevant to this work [37].

3.1 Interatomic potential

The choice of interatomic potential used for ortho-deuterium and hydrogen deuteride is the Silvera-Goldman potential [38], in which the molecules are treated at spherical particles. The Silver-Goldman potential assumes that the isotopic hydrogen molecules remain in the rotational ground state, which is satisfied at the temperatures, 17 K and 20 K, used in this report. The Silvera-Goldman potential, as shown in Equation 3.1, is commonly used for both H_2 and D_2 [39][22]. While the Silvera-Goldman potential has been used to calculate static properties of hydrogen deuteride [40], it has not been used, to our knowledge, for calculating the velocity auto-correlation function of hydrogen deuteride. The potential is given by

$$V(r) = e^{\alpha_c - \beta_c r - \gamma_c r^2} - \left(\frac{C_6}{r^6} + \frac{C_8}{r^8} - \frac{C_9}{r^9} + \frac{C_{10}}{r^{10}}\right) f_c(r), \tag{3.1}$$

where r is the distance between atoms, and

$$f_c(r) = \begin{cases} e^{-(r_c/r-1)^2}, & \text{if } r \leq r_c \\ 1, & \text{otherwise.} \end{cases} \tag{3.2}$$

The parameters for Equations 3.1 and 3.2 are listed in Table 1.

a_c	1.713	C_6	12.14
β_c	1.5671	C_8	215.2
γ_c	0.00993	C_9	143.1
r_c	8.32	C_{10}	4812.9

Table 1: Parameters used for the Silvera-Goldman potential, given in atomic units [38][41].

3.2 Initial configuration

In order to begin the molecular dynamics simulation, a set of initial properties are defined. Such properties include the number of particles, the density of the system, as well as the initial positions and velocities of the molecules. While liquids do not take the shape of a crystal lattice, the option of randomly distributed molecules is not preferable as multiple molecules can be initiated on top of each other, which would add additional potential energy to the system. For this reason, the systems used in this work were initiated with a cubic lattice. The boundaries of the system were set to periodic, which allows a particle reaching the boundaries to appear on the opposite side with the same velocity. This allows smaller systems to behave approximately as a part of a larger system without the increased computational requirements. The initial velocity of the molecules were taken from a Maxwell-Boltzmann distribution at the desired initial temperature [42].

3.3 Equilibrium run

The initial configuration of the system is unlikely to be in equilibrium and has to be run through an equilibrium simulation in which the system is progressed through time and average quantities such as kinetic energy, pressure, potential energy, and temperature progress towards an equilibrium. It is not uncommon to carry out molecular dynamics simulations in an NVE ensemble in which the number of particles, N, the volume, V, and the total energy, E, are conserved in each time step. However this can be problematic in our case since we are interested in a particular temperature rather than a particular total energy. Since the initial configuration of the system is not in equilibrium, the temperature is likely to drift away from the desired value. In order to preserve the temperature of interest, the system uses an NVT ensemble in which the temperature, T, is conserved in each time step rather than the energy. Such an ensemble can be seen as a smaller system exchanging energy with a larger system. A common choice for the NVT setup is to use the Langevin thermostat [42] in which the system moves through a continuum of smaller particles which creates a damping force on the system particles. The smaller particles also have thermal motion which allows them to occasionally transfer part of their energy to the system particles. This occasional energy deposit, along with the damping force keeps the system in a NVT ensemble.

3.4 Static structure factor

The static structure factor, $S(Q)$, used for the Sköld approximation in the NJOY-H2D2 version of LEAPR module, is calculated using the pair distribution function, $g(r)$. The static structure factor is given by

$$S(Q) = 1 + \frac{4\pi\rho}{Q}\int_0^\infty rsin(Qr)h(r)dr, \tag{3.3}$$

where ρ is the density, and $h(r) = g(r) - 1$ [43]. The pair distribution function can be obtained by using the TRAVIS software [44][45]. This is done by inputting the trajectory run file(s) obtained from the equilibrium run. Depending on the amount of time available and the accuracy needed, one can either obtain the pair distribution function using the trajectory of the centroids of the molecules, or by using the trajectory of each bead used to approximate the molecules and taking an average of all of them. These methods will be referred to as the 'centroids' and 'beads' methods in this paper. The 'beads' method has shown better agreement with experimental data [31][32]. Since the size of the system simulated in molecular dynamics is somewhat limited, the pair distribution function has to be extrapolated to longer distances in order to accurately represent a larger system. The extrapolation is done using an oscillating dampened function [43],

$$h(r) = \frac{A_0}{r}e^{\frac{r}{r_0}}sin\left(\frac{r}{r_1}\right) \tag{3.4}$$

where the parameters A_0, r_0, and r_1 are obtained by fitting the function to the pair distribution function between a few zero crossings.

3.5 Velocity auto-correlation function

When the equilibrium run is completed, the average quantities are assessed to ensure that the system reached equilibrium. Once that is done, the system is moved over to the NVE ensemble and the particle trajectories are recorded and later used to calculate the velocity auto-correlation function. In order to

reach a statistical certainty, the particle trajectory is sampled over 100 runs and an average of those runs is calculated.

The velocity auto-correlation function (VACF), $u(t)$, describes the correlation of a particle's velocity at time $t_0 + t$ compared to its velocity at time t_0. The VACF is calculated over a number of atoms, N, and is given by

$$u(t) = \langle \vec{v}_i(t + t_0) \cdot \vec{v}_i(t_0) \rangle = \sum_{t_0} \sum_{i=0}^{N-1} \vec{v}_i(t + t_0) \cdot \vec{v}_i(t_0), \tag{3.5}$$

where $\vec{v}_i$ is the velocity of the i-th atom. However to be more precise, the output obtained through PIMD is the canonical (or kubo-transformed) VACF which is a real and even function with regards to time, unlike the VACF which is a complex function [13]. The canonical VACF is given by

$$u_c(t) = \frac{1}{\beta} \int_0^\beta d\lambda \left\langle e^{\lambda H} \vec{v}_{c.m}(0) \cdot e^{-\lambda H} \vec{v}_{c.m}(t) \right\rangle, \tag{3.6}$$

where $\vec{v}_{c.m}$ denotes the center of mass velocity vector, H is the Hamiltonian operator of the system and $\beta = (k_B T)^{-1}$. The frequency distribution of the canonical VACF, $\rho_c(\omega)$, can then be used to obtain the frequency distribution of the VACF, $\rho(\omega)$, and is given by

$$\rho_c(\omega) = \frac{1}{2\pi} \int_{-\infty}^{\infty} u_c(t) e^{-i\omega t} dt, \tag{3.7}$$

and

$$\rho(\omega) = \rho_c(\omega) \frac{\beta_T \hbar \omega}{1 - e^{-\beta_T \hbar \omega}}. \tag{3.8}$$

Not only can the canonical frequency distribution of the VACF be used to validate the RPMD results, it is also used in order to obtain the frequency spectrum, $f(\omega)$, as given by

$$f(\omega) = \frac{2m\beta T}{3} \rho_c(\omega) = \frac{m\beta T}{3\pi} \int_{-\infty}^{\infty} u_c(t) e^{-i\omega t} dt. \tag{3.9}$$

It can be noted that in literature, different frequency spectra can be presented. For example, $\rho(\omega)$ could be shown instead of $\rho_c(\omega)$.

3.6 Diffusion component

In order to calculate the translational part of the dynamic structure factor, see Section 2.3, it is separated into two parts, a solid-like (phonon) component and a diffusion component. Both of these components require their corresponding frequency spectrum. This is done by dividing the frequency spectrum obtained through RPMD into a solid-like component (phonon distribution), $f_{solid}(\omega)$ and a diffusion component, $f_{diff}(\omega)$, and is given by

$$f(\omega) = f_{solid}(\omega) + f_{diff}(\omega). \tag{3.10}$$

The diffusion component of the frequency spectrum is obtained by using the diffusion model by Egelstaff and Schofield [25], which has a frequency spectrum given by

$$f_{diff}(\omega) = \frac{4p\omega_t}{\pi} \sqrt{p^2 + \frac{1}{4}} \sinh\left(\frac{\beta}{2}\right) K_1\left(\beta \sqrt{p^2 + \frac{1}{4}}\right), \tag{3.11}$$

where w_t is the weight of the diffusion component, $K_1(x)$ is the modified Bessel function of the second kind, and p is the dimensionless diffusion coefficient given by

$$p = \frac{mD}{w_t \hbar}, \tag{3.12}$$

where D is the diffusion constant and is given by

$$D = \frac{1}{3} \int_0^\infty u_c(t) dt. \tag{3.13}$$

4 Results and Discussion

All of the RPMD simulations were done using a cubic box with periodic boundary conditions. The system was initiated using a cubic crystal structure and the velocities were spread out according to a Boltzmann distribution. The system was first run in an NVT setting until it reached an equilibrium state. The system was then run through an NVE setting and the trajectories were recorded for a series of simulations. Afterwards, the canonical VACF was calculated as an average over the trajectories obtained in the NVE simulations. The static structure function was then calculated with the pair correlation function obtained using the TRAVIS code with the trajectories from the NVE simulations [44][45].

4.1 Ortho-deuterium

The RPMD simulations done for ortho-deuterium were run at a temperature of 20 K.

4.1.1 Static structure factor

In order to calculate the static structure factor, $S(Q)$, Equation 3.3 was used and the pair distribution function, $g(r)$, was obtained through analysis using TRAVIS in conjunction with trajectory outputs from molecular dynamics simulations [44][45]. In order to obtain high statistical certainty, the molecular dynamics simulations were run with a system of 4096 molecules. The number of beads used to simulate the molecules was chosen to be 64, and while this increased the simulation time, it was done to get a more accurate pair distribution function, and in turn a more accurate static structure function. The pair distribution function was fitted between 500 pm and 1300 pm as shown in Figure 1a, and extended to 70 nm, using an exponentially decaying sine function in order to prevent a sudden edge to zero, as shown in Figure 1b. The smoothing function used in Figure 1b is the following, $y = y_d(a-x)/a + y_f x/a$, where y_d is the data, y_f is fitted function and a is the number of data points being smoothed. The static structure function is shown in Figure 2 along with experimental data from Zoppi et al[46]. The static structure function was calculated in two ways, using the pair distribution function calculated with the centroids of the molecules, and using the mean of the pair distribution calculated for each individual bead. The 'beads' method shows strong agreement to the experimental values of Zoppi [46], and was thus used to calculate the neutron cross section.

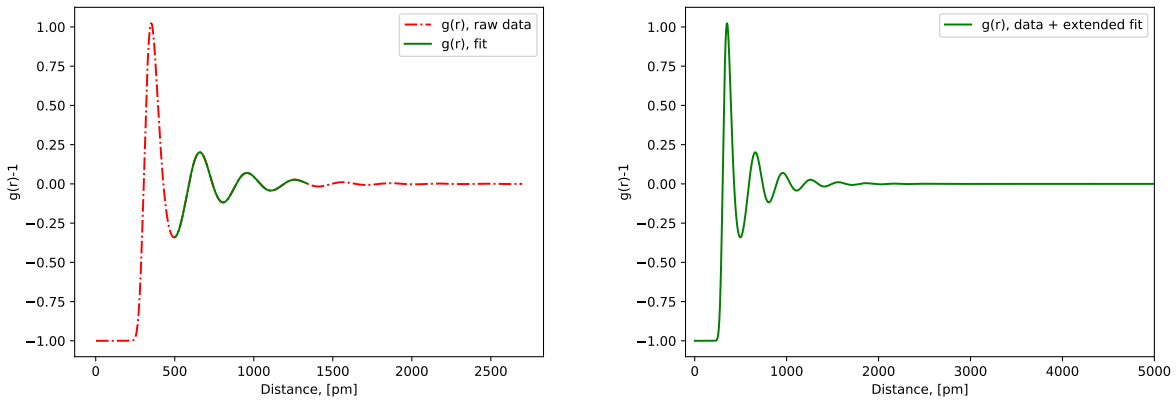

(a) (b)

Figure 1: a) The pair distribution function of ortho-deuterium calculated using the 'beads' method, along with a fitted exponentially decaying sine function between 500 pm and 1300 pm. b) The extended pair distribution function of ortho-deuterium calculated using the 'beads' method. The function uses the raw data up until 500 pm, upon which a smoothing function is used for 10 data points, after which the exponentially decaying sinus function, seen in Figure 1a, is used to extend the pair distribution function to 70 nm.

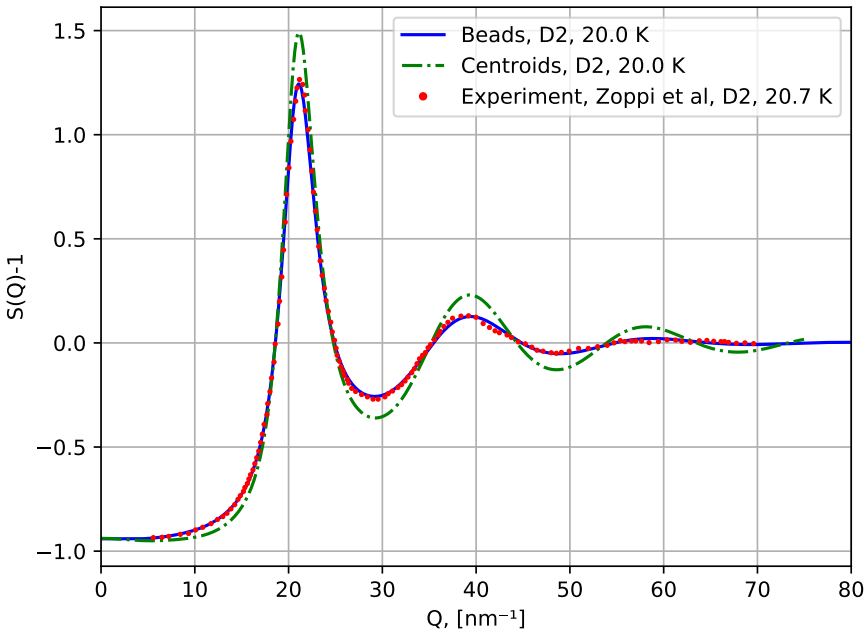

Figure 2: Static structure factor of ortho-deuterium at 20 K, n=25.6 nm^{-3}, calculated using the centroids and 'beads' method, compared to experimental data points from Zoppi [46].

4.1.2 Velocity auto-correlation function

The canonical VACF was computed as an average of 64 trajectory runs of 16 ps with a system size of 343 molecules. The canonical VACF was compared to simulations done by Guarini et al. using CMD [22], as shown in Figure 3. There are no notable differences between these results and those of Guarini et al.

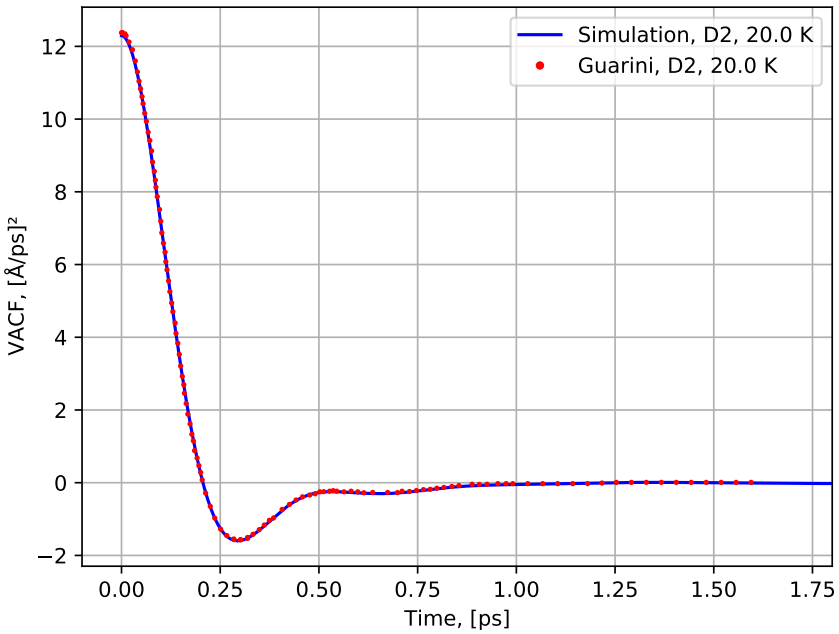

Figure 3: Canonical VACF of ortho-deuterium at 20 K and $\rho = 25.6$ nm^{-3}, obtained through RPMD compared to results by Guarini et al. (CMD) [22].

4.1.3 Frequency distribution

The frequency distribution, $\rho(\omega)$, was calculated using the VACF using Equations 3.8-3.7. The frequency spectrum, $f(\omega)$, was then calculated using Equation 3.9. These results were then compared to previous experiments and simulations. Figure 4 shows the calculated frequency distribution along with CMD simulation results by Hone and Voth [39], obtained at 20.7 K. While there are minor disagreements in Figure 4 at tails of the function, the overall deviations remain small despite the slight temperature difference. The frequency spectrum was compared to experimental data by Colognesi et al. [47] and is shown in Figure 5. The calculations by Colognesi et al. were also carried out using the method of CMD, which could be a possible reason for the differences. The diffusion component of the frequency spectrum was calculated using Equation 3.11, and then subtracted from the frequency spectrum, as shown in Figure 6, in order to obtain the solid-like phonon distribution, $\rho_{solid}(\omega)$, which is used as an input for LEAPR.

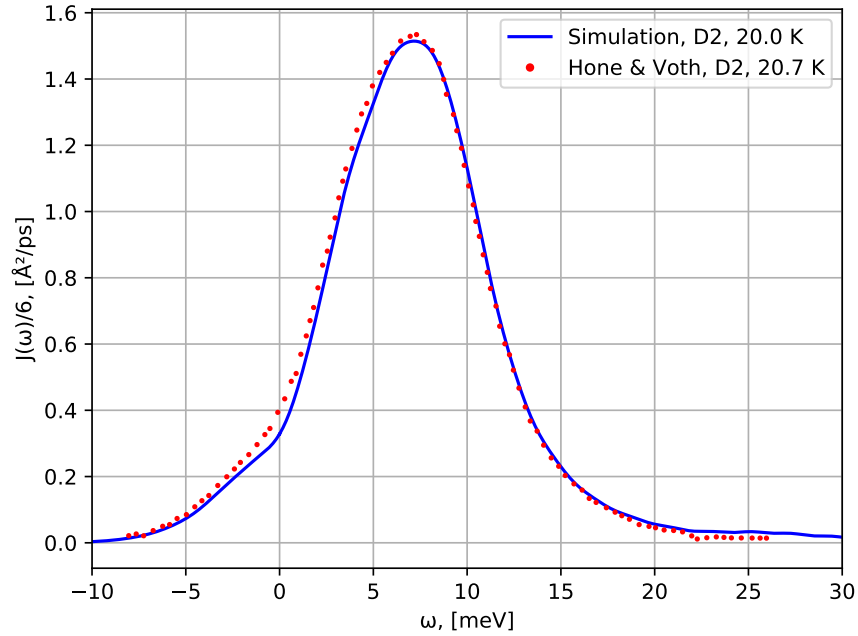

Figure 4: Frequency distribution of the VACF, for ortho-deuterium at 20 K, calculated using Equation 3.8, and compared to results by Hone and Voth, at 20.7 K [39].

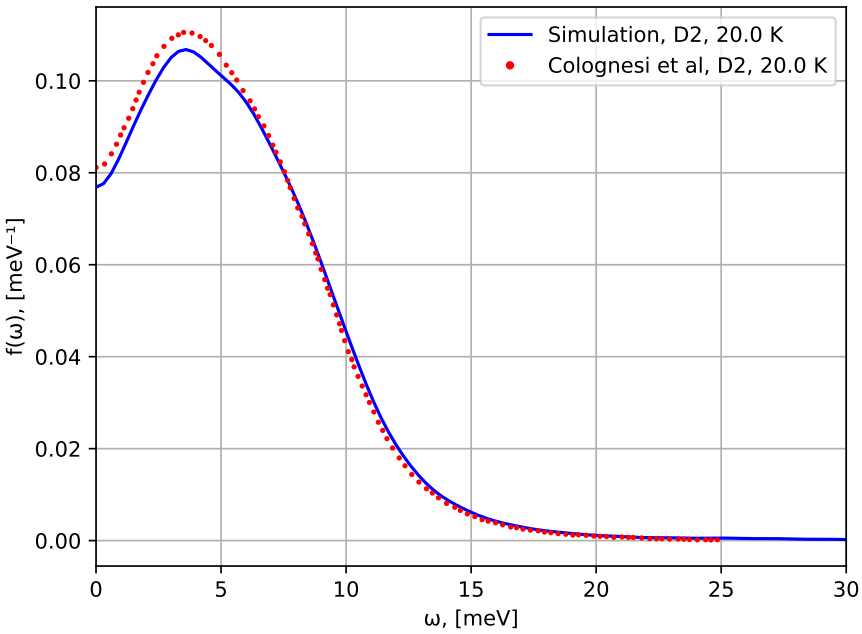

Figure 5: Frequency spectrum of ortho-deuterium calculated using Equation 3.9, and compared to experimental data points by Colognesi et al. [47].

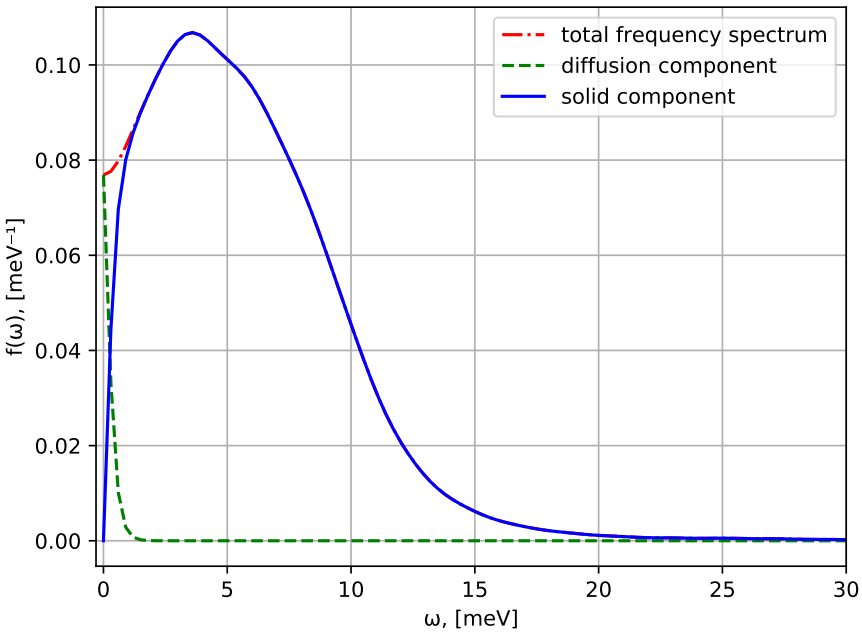

Figure 6: Frequency spectrum of ortho-deuterium, at 20 K, along with the diffusion component calculated using Equation 3.11, and the resulting phonon distribution.

4.1.4 Total inelastic cross-section

The total inelastic cross section was calculated with NJOY using the phonon distribution, static structure factor, and the diffusion constant, all obtained through molecular dynamics simulations.The NJOY-H2D2 code [10] was used for the calculations.

The total inelastic cross section was then compared to simulation results from Jeff 3.3 [9], Guarini et al. [22], and experimental data from Seiffert [48], and plotted in Figure 7. When comparing to the previous simulations and experimental data, it is clear that the new method can be used in order to produce an accurate total inelastic cross-section, for ortho-deuterium, using quantum molecular dynamics. While there is a slight difference in the low energy tail, the overall curve agrees well with both experimental data and simulations. While the experimental data was obtained for 19 K, and the current simulation in Figure 7 is for 20 K, it can be seen that the only notable difference between the 19 K and 20 K simulations is the low energy tail, with the 20 K tail rising faster than the 19 K one. Although the simulation overestimates the cross-section in the intermediate energy region, the same behaviour can be seen for the other simulations presented in the plot.

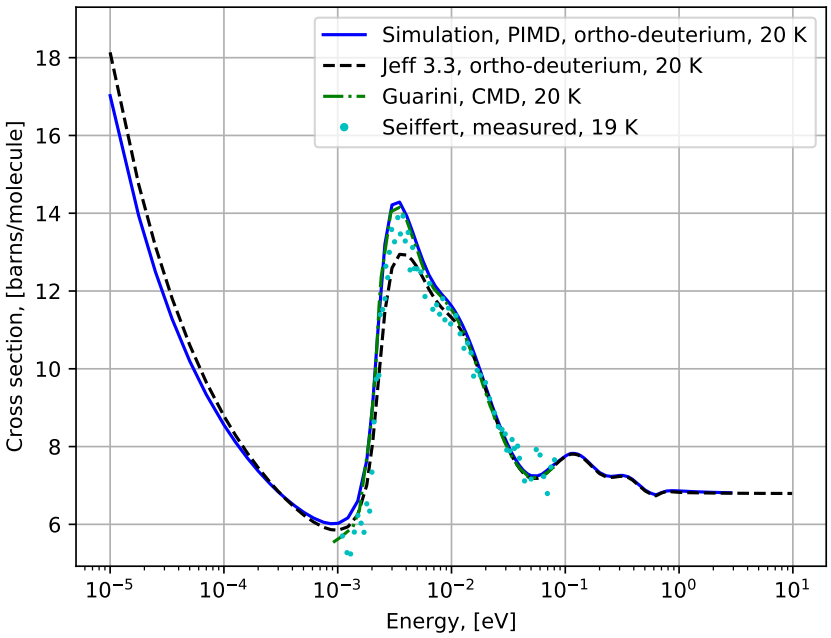

Figure 7: The total inelastic cross-section of ortho-deuterium calculated through NJOY with inputs from RPMD, and compared to both experimental and simulated results [48][22].

4.2 Hydrogen deuteride

The RPMD simulations done for hydrogen deuteride were run at a temperature of 17 K.

4.2.1 Static structure factor

The structure factor, $S(Q)$, was calculated in the same way as for ortho-deuterium using Equation 3.3, and the pair distribution function, $g(r)$, was obtained through TRAVIS using results from molecular dynamics simulations as input [44][45]. The molecular dynamics simulations were run for a system of 4096 molecules, and each molecule consisting of 64 beads in order to obtain more accurate results. The pair distribution function was fitted between 500 pm and 1300 pm using an exponentially decaying sine function, as shown in Figure 8a, and extended to 70 nm, as shown in Figure 8b, in order to prevent a sudden edge to zero. The smoothing function used in Figure 8b is the following, $y = y_d(a-x)/a + y_f x/a$, where y_d is the data, y_f is fitted function and a is the number of data points being smoothed. The static structure function is shown in Figure 9. As the static structure factor of ortho-deuterium showed better agreement with experimental data using the 'beads' method, it also became the method of choice for the NJOY input of hydrogen deuteride as well.

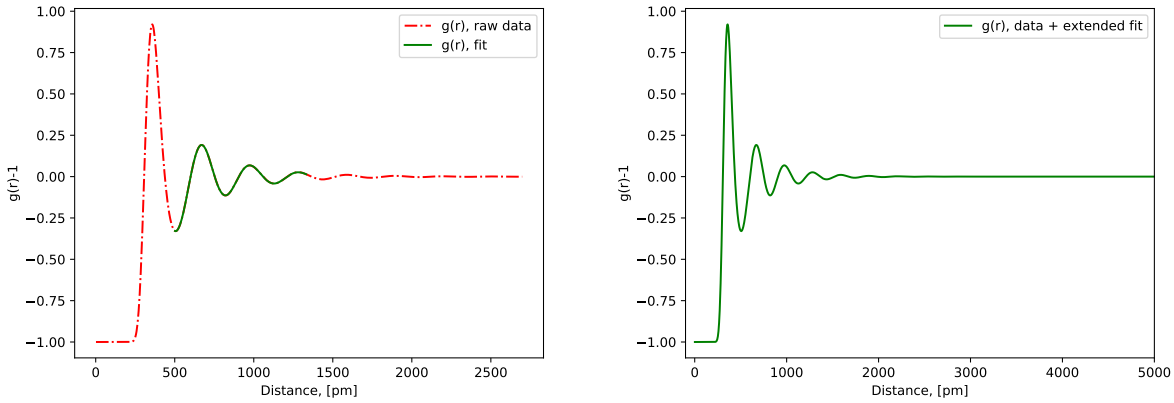

(a) (b)

Figure 8: a) The pair distribution function of hydrogen deuteride calculated using the 'beads' method, along with a fitted exponentially decaying sine function between 500 pm and 1300 pm. b) The extended pair distribution function of hydrogen deuteride calculated using the 'beads' method. The function uses the raw data up until 500 pm, upon which a smoothing function is used for 10 data points, after which the exponentially decaying sinus function, seen in Figure 8a, is used to extend the pair distribution function to 70 nm.

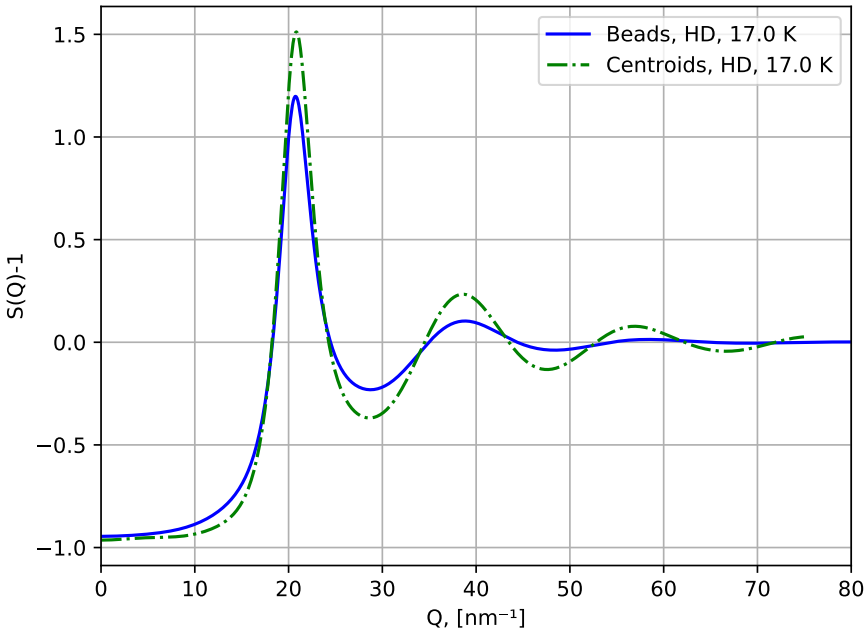

Figure 9: Static structure factor of hydrogen deuteride at 17 K, $\rho = 24.37$ nm^{-3}, calculated using the centroids and 'beads' method.

4.2.2 Velocity auto-correlation function

The canonical VACF was computed as an average of 64 trajectory runs of 16 ps with a system size of 216 molecules.

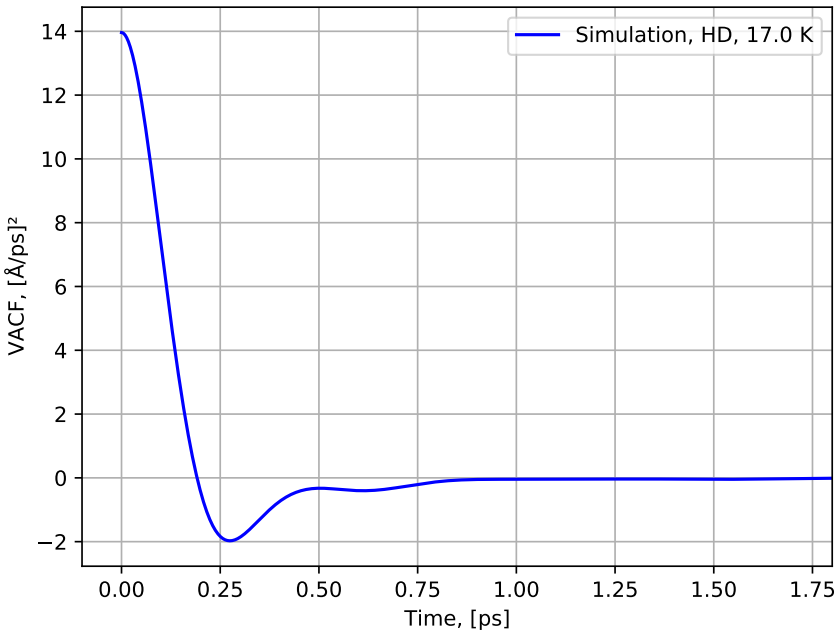

Figure 10: Canonical VACF of hydrogen deuteride at 17 K and $\rho = 24.37$ nm^{-3}, obtained through RPMD.

4.2.3 Frequency distribution

The frequency distribution, $\rho(\omega)$, was calculated using the VACF using Equations 3.8-3.7. The frequency spectrum, $f(\omega)$, was then calculated using Equation 3.9. Figure 11 shows the calculated frequency distribution. The frequency spectrum is shown in Figure 12. The diffusion component of the frequency spectrum was calculated using Equation 3.11, and then subtracted from the frequency spectrum, as shown in Figure 13, in order to obtain the solid-like phonon distribution, $\rho_{solid}(\omega)$, which is used as an input for LEAPR.

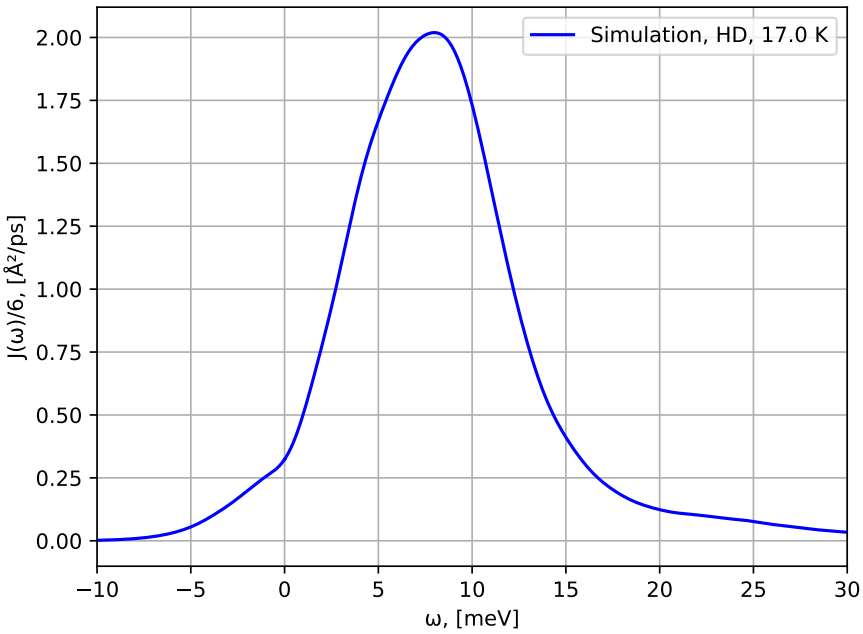

Figure 11: Frequency distribution of the VACF, for hydrogen deuteride at 17 K, calculated using Equation 3.8.

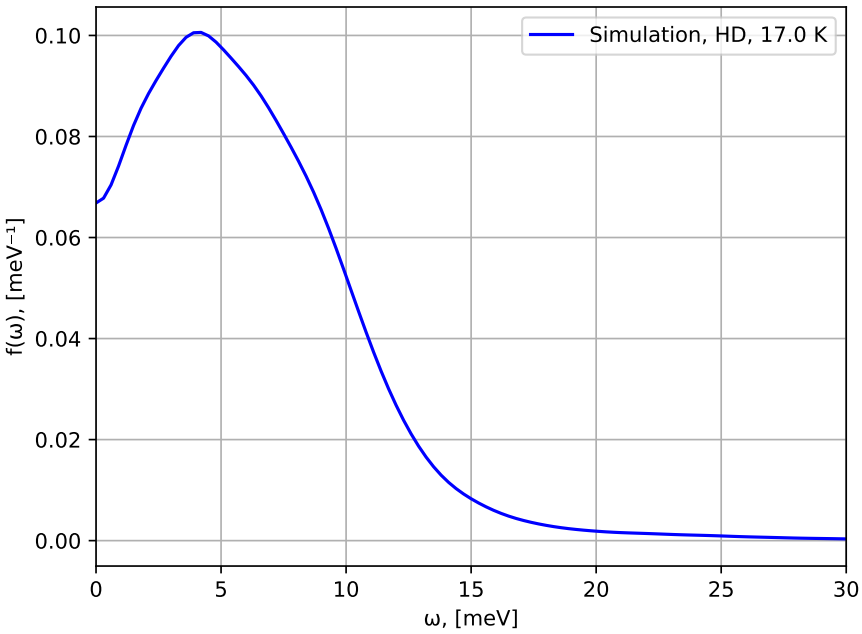

Figure 12: Frequency spectrum of hydrogen deuteride calculated using Equation 3.9.

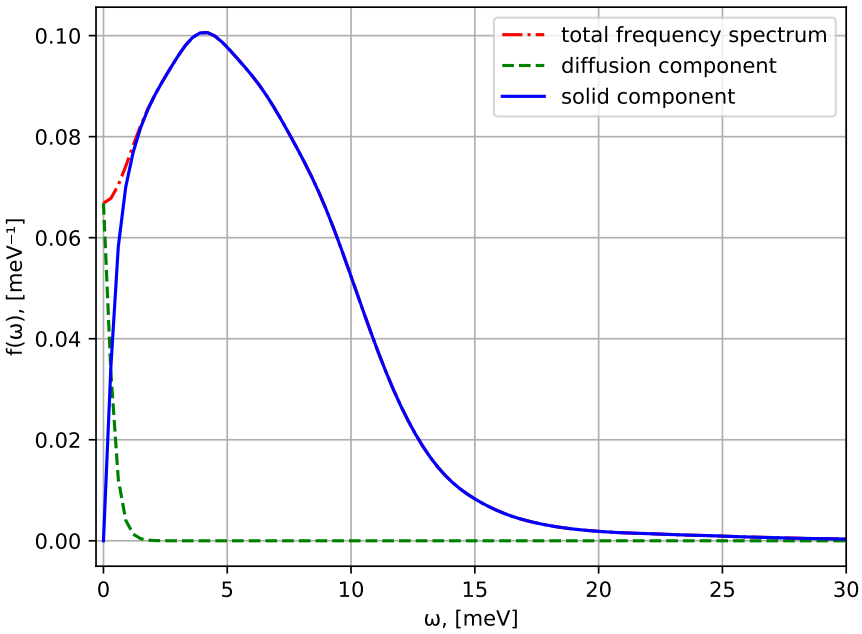

Figure 13: Frequency spectrum of hydrogen deuteride, at 17 K, along with the diffusion component calculated using Equation 3.11, and the resulting phonon distribution.

4.2.4 Total inelastic cross-section

The total inelastic cross section was calculated with NJOY using the phonon distribution, static structure factor, and the diffusion constant, all obtained through molecular dynamics simulations. NJOY was not developed to handle heterogeneous molecules. The NJOY-H2D2 code [10] was used and developed to include the additional terms in Equations 2.22-2.24 for HD. Furthermore, the statistical weight function had to be adjusted as hydrogen deuteride does not have spin correlation which is implemented in NJOY-H2D2. In addition, the total inelastic scattering was computed using two NJOY-H2D2 input files. In the case of D_2, this is not required as the scattering is assigned to solely the D atom. For HD, the total cross-section was computed from the sum of the partial cross-sections resulting from the scattering contributions assigned to the H and D atoms individually. The normalization had to be adjusted as we modified the code to run two separate files with the hydrogen and deuterium atom contributions to the hydrogen deuteride cross section. The calculations presented here do not include the contribution from the distinct term of the dynamic structure factor.

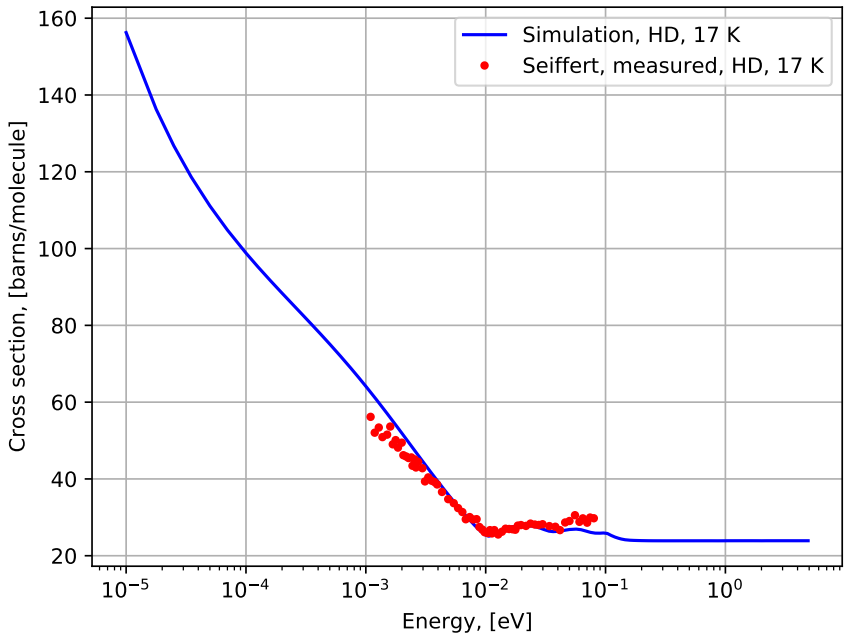

Figure 14: The total inelastic cross-section of hydrogen deuteride calculated through NJOY with inputs from RPMD, and compared to experimental data [48].

5 Summary and Outlook

In this work, path integral molecular dynamics techniques were used to simulate multiple properties of ortho-deuterium, which include the frequency distribution, static structure factor, and cross section. Furthermore, it has been shown that it is possible to derive these quantities for hydrogen deuteride, using the rotational part from previous models described in literature, combined with a translational component which represents the liquid behaviour. The results obtained for hydrogen deuteride are promising especially since this is the first time a scattering library has been generated for hydrogen deuteride. Future work could include investigating the impact of the distinct part for hydrogen deuteride as well as the implementation of it in the modified version of NJOY-H2D2. Furthermore, it would be of interest to look into solid hydrogen deuteride and solid deuterium as potential cold neutron moderators. Another way to move forward would be to use the generated libraries in Monte-Carlo simulations and compare the emission spectra of hydrogen deuteride, ortho-deuterium, and para-hydrogen to get a better understanding of their moderating properties. The results obtained in this study form a basis for future work on these materials that may be presented at conferences or in publications.

References

[1] Roland Garoby et al. "The European Spallation Source Design". In: *Physica Scripta* 93 (Dec. 2018), p. 014001. DOI: 10.1088/1402-4896/aa9bff.

[2] L. Zanini et al. "Design of the cold and thermal neutron moderators for the European Spallation Source". In: *Nuclear Instruments and Methods in Physics Research Section A: Accelerators, Spectrometers, Detectors and Associated Equipment* 925 (2019), pp. 33–52. ISSN: 0168-9002. DOI: https://doi.org/10.1016/j.nima.2019.01.003. URL: https://www.sciencedirect.com/science/article/pii/S0168900219300087.

[3] European Spallation Source, "Home page", European Spallation Source, https://europeanspallationsource.se/, Accessed on: August 26, 2021.

[4] Esben Klinkby et al. *Voluminous D2 source for intense cold neutron beam production at the ESS*. 2014. arXiv: 1401.6003 [physics.ins-det].

[5] V. Santoro et al. "Development of high intensity neutron source at the European Spallation Source". English. In: *Journal of Neutron Research* 22.2-3 (2020), pp. 209–219. ISSN: 1023-8166. DOI: 10.3233/JNR-200159.

[6] Robert Macfarlane et al. "The NJOY Nuclear Data Processing System, Version 2016". In: (Jan. 2017). DOI: 10.2172/1338791. URL: https://www.osti.gov/biblio/1338791.

[7] J. I. Márquez Damián. ""NJOY H2D2, Git page." GitHub, Accessed on: August 26, 2021". In: (). URL: https://github.com/marquezj/NJOY2016/tree/H2D2.

[8] J.R. Granada and V.H. Gillette. "A new thermal neutron scattering kernel for liquid hydrogen". In: *Physica B: Condensed Matter* 348.1 (2004), pp. 6–14. ISSN: 0921-4526. DOI: https://doi.org/10.1016/j.physb.2003.07.008. URL: https://www.sciencedirect.com/science/article/pii/S0921452603006434.

[9] Nuclear Energy Agency, "jeff-3.3", Nuclear Energy Agency. [Website] Available: https://www.oecd-nea.org/dbdata/jeff/jeff33/index.html. Accessed on: December 9, 2021.

[10] *Thermal Scattering Law S(α,β): Measurement, Evaluation and Application-International Evaluation Co-operation Volume 42*. 2020.

[11] J.I. Márquez Damián, J.R. Granada, and D.C. Malaspina. "CAB models for water: A new evaluation of the thermal neutron scattering laws for light and heavy water in ENDF-6 format". In: *Annals of Nuclear Energy* 65 (2014), pp. 280–289. ISSN: 0306-4549. DOI: https://doi.org/10.1016/j.anucene.2013.11.014. URL: https://www.sciencedirect.com/science/article/pii/S0306454913005987.

[12] J.I. Márquez Damián et al. "Generation of thermal scattering libraries for liquids beyond the Gaussian approximation using molecular dynamics and NJOY/LEAPR". In: *Annals of Nuclear Energy* 92 (2016), pp. 107–112. ISSN: 0306-4549. DOI: https://doi.org/10.1016/j.anucene.2016.01.036. URL: https://www.sciencedirect.com/science/article/pii/S0306454916300469.

[13] E. Guarini et al. "Velocity autocorrelation in liquid parahydrogen by quantum simulations for direct parameter-free computations of neutron cross sections". In: *Phys. Rev. B* 92 (10 Sept. 2015), p. 104303. DOI: 10.1103/PhysRevB.92.104303. URL: https://link.aps.org/doi/10.1103/PhysRevB.92.104303.

[14] Thomas F. Miller and David E. Manolopoulos. "Quantum diffusion in liquid para-hydrogen from ring-polymer molecular dynamics". In: *The Journal of Chemical Physics* 122.18 (2005), p. 184503. DOI: 10.1063/1.1893956. eprint: https://doi.org/10.1063/1.1893956. URL: https://doi.org/10.1063/1.1893956.

[15] Pontus Nordin. "Scattering Kernel Calculations for Liquid Para-Hydrogen Using Ring Polymer Molecular Dynamics". eng. In: (2020). Student Paper.

[16] Jose Ignacio Marquez Damian, Douglas Dijulio, and Guenter Muhrer. "Nuclear data development at the European Spallation Source". In: *Journal of Neutron Research* 23 (May 2021), pp. 1–10. DOI: 10.3233/JNR-210014.

[17] G. I. Bell and S. Glasstone. "Nuclear Reactor Theory". In: (Oct. 1970). URL: https://www.osti.gov/biblio/4074688.

[18] G. L. Squires. "Introduction to the Theory of Thermal Neutron Scattering." In: (1996). URL: https://www.osti.gov/biblio/4074688.

[19] James A. Young and Juan U. Koppel. "Slow Neutron Scattering by Molecular Hydrogen and Deuterium". In: *Phys. Rev.* 135 (3A Aug. 1964), A603–A611. DOI: 10.1103/PhysRev.135.A603. URL: https://link.aps.org/doi/10.1103/PhysRev.135.A603.

[20] Eleonora Guarini. *The neutron cross section of low-temperature heteronuclear diatomic fluids*. 2021. arXiv: 2107.05422 [cond-mat.other].

[21] Kurt Sköld. "Small Energy Transfer Scattering of Cold Neutrons from Liquid Argon". In: *Phys. Rev. Lett.* 19 (18 Oct. 1967), pp. 1023–1025. DOI: 10.1103/PhysRevLett.19.1023. URL: https://link.aps.org/doi/10.1103/PhysRevLett.19.1023.

[22] E. Guarini et al. "Velocity autocorrelation by quantum simulations for direct parameter-free computations of the neutron cross sections. II. Liquid deuterium". In: *Phys. Rev. B* 93 (22 June 2016), p. 224302. DOI: 10.1103/PhysRevB.93.224302. URL: https://link.aps.org/doi/10.1103/PhysRevB.93.224302.

[23] Y. Abe, T. Tsuboi, and S. Tasaki. "Evaluation of the neutron scattering cross-section for light water by molecular dynamics". In: *Nuclear Instruments and Methods in Physics Research Section A: Accelerators, Spectrometers, Detectors and Associated Equipment* 735 (2014), pp. 568–573. ISSN: 0168-9002. DOI: https://doi.org/10.1016/j.nima.2013.10.024. URL: https://www.sciencedirect.com/science/article/pii/S0168900213013703.

[24] Gordon Leslie Squires. *Introduction to the theory of thermal neutron scattering*. Cambridge University Press, 2012.

[25] P. A. Egelstaff and P. Schofield. "On the Evaluation of the Thermal Neutron Scattering Law". In: *Nuclear Science and Engineering* 12.2 (1962), pp. 260–270. DOI: 10.13182/NSE62-A26066. eprint: https://doi.org/10.13182/NSE62-A26066. URL: https://doi.org/10.13182/NSE62-A26066.

[26] National Institute of Standard and Technology, "deuterium", National Institute of Standard and Technology. [Website] Available: https://webbook.nist.gov/cgi/cbook.cgi?ID=7782-39-0. Accessed on: December 9, 2021.

[27] National Institute of Standard and Technology, "deuterium hydride", National Institute of Standard and Technology. [Website] Available: https://webbook.nist.gov/cgi/cbook.cgi?ID=C13983205. Accessed on: December 9, 2021.

[28] R. G. Sachs and E. Teller. "The Scattering of Slow Neutrons by Molecular Gases". In: *Phys. Rev.* 60 (1 July 1941), pp. 18–27. DOI: 10.1103/PhysRev.60.18. URL: https://link.aps.org/doi/10.1103/PhysRev.60.18.

[29] Eleonora Guarini. "The neutron double differential cross-section of simple molecular fluids: refined computing models and nowadays applications". In: *Journal of Physics: Condensed Matter* 15.19 (May 2003), R775–R812. DOI: 10.1088/0953-8984/15/19/204. URL: https://doi.org/10.1088/0953-8984/15/19/204.

[30] Norman A. Lurie. "Influence of Rotational Levels on Slow-Neutron Scattering by Linear Gases". In: *The Journal of Chemical Physics* 46.1 (1967), pp. 352–356. DOI: 10.1063/1.1840393. eprint: https://doi.org/10.1063/1.1840393. URL: https://doi.org/10.1063/1.1840393.

[31] Francico Bermejo et al. "Beyond classical molecular dynamics: Simulation of quantum-dynamics effects at finite temperatures; The case of condensed molecular hydrogen". In: *Chemical Physics* 317 (Oct. 2005), pp. 198–207. DOI: 10.1016/j.chemphys.2005.04.010.

[32] Nicholas Blinov and Pierre-Nicholas Roy. "Connection between the observable and centroid structural properties of a quantum fluid: Application to liquid para-hydrogen". In: *The Journal of Chemical Physics* 120.8 (2004), pp. 3759–3764. DOI: 10.1063/1.1642600. eprint: https://doi.org/10.1063/1.1642600. URL: https://doi.org/10.1063/1.1642600.

[33] Richard Phillips Feynman and Albert Roach Hibbs. *Quantum mechanics and path integrals*. International series in pure and applied physics. New York, NY: McGraw-Hill, 1965. URL: https://cds.cern.ch/record/100771.

[34] Jianshu Cao and Gregory A. Voth. "The formulation of quantum statistical mechanics based on the Feynman path centroid density. V. Quantum instantaneous normal mode theory of liquids". In: *The Journal of Chemical Physics* 101.7 (1994), pp. 6184–6192. DOI: 10.1063/1.468400. eprint: https://doi.org/10.1063/1.468400. URL: https://doi.org/10.1063/1.468400.

[35] Ian R. Craig and David E. Manolopoulos. "Inelastic neutron scattering from liquid para-hydrogen by ring polymer molecular dynamics". In: *Chemical Physics* 322.1 (2006). Real-time dynamics in complex quantum systems, pp. 236–246. ISSN: 0301-0104. DOI: https://doi.org/10.1016/j.chemphys.2005.07.012. URL: https://www.sciencedirect.com/science/article/pii/S0301010405002995.

[36] Venkat Kapil et al. "i-PI 2.0: A universal force engine for advanced molecular simulations". In: *Computer Physics Communications* 236 (2019), pp. 214–223. ISSN: 0010-4655. DOI: https://doi.org/10.1016/j.cpc.2018.09.020. URL: https://www.sciencedirect.com/science/article/pii/S0010465518303436.

[37] Tyler D. Hone, Peter J. Rossky, and Gregory A. Voth. "A comparative study of imaginary time path integral based methods for quantum dynamics". In: *The Journal of Chemical Physics* 124.15 (2006), p. 154103. DOI: 10.1063/1.2186636. eprint: https://doi.org/10.1063/1.2186636. URL: https://doi.org/10.1063/1.2186636.

[38] Isaac F. Silvera and Victor V. Goldman. "The isotropic intermolecular potential for H2 and D2 in the solid and gas phases". In: *The Journal of Chemical Physics* 69.9 (1978), pp. 4209–4213. DOI: 10.1063/1.437103. eprint: https://doi.org/10.1063/1.437103. URL: https://doi.org/10.1063/1.437103.

[39] Tyler D. Hone and Gregory A. Voth. "A centroid molecular dynamics study of liquid para-hydrogen and ortho-deuterium". In: *The Journal of Chemical Physics* 121.13 (2004), pp. 6412–6422. DOI: 10.1063/1.1780951. eprint: https://doi.org/10.1063/1.1780951. URL: https://doi.org/10.1063/1.1780951.

[40] D. Colognesi et al. "Lattice dynamics and molecular rotations in solid hydrogen deuteride: Inelastic neutron scattering study". In: *Phys. Rev. B* 79 (14 Apr. 2009), p. 144307. DOI: 10.1103/PhysRevB.79.144307. URL: https://link.aps.org/doi/10.1103/PhysRevB.79.144307.

[41] Wilfried Meyer. "Dynamic multipole polarizabilities of H2 and He and long-range interaction coefficients for H2-H2,H2He and He-He". In: *Chemical Physics* 17.1 (1976), pp. 27–33. ISSN: 0301-0104. DOI: https://doi.org/10.1016/0301-0104(76)85004-5. URL: https://www.sciencedirect.com/science/article/pii/0301010476850045.

[42] R. Lesar. "Introduction to Computational Materials Science, Fundamentals to Applications". In: (2013).

[43] M. Celli et al. "Microscopic structure factor of liquid hydrogen by neutron-diffraction measurements". In: *Phys. Rev. B* 71 (1 Jan. 2005), p. 014205. DOI: 10.1103/PhysRevB.71.014205. URL: https://link.aps.org/doi/10.1103/PhysRevB.71.014205.

[44] Martin Brehm and Barbara Kirchner. "TRAVIS - A Free Analyzer and Visualizer for Monte Carlo and Molecular Dynamics Trajectories". In: *Journal of Chemical Information and Modeling* 51.8 (2011). PMID: 21761915, pp. 2007–2023. DOI: 10.1021/ci200217w. eprint: https://doi.org/10.1021/ci200217w. URL: https://doi.org/10.1021/ci200217w.

[45] M. Brehm et al. "TRAVIS—A free analyzer for trajectories from molecular simulation". In: *The Journal of Chemical Physics* 152.16 (2020), p. 164105. DOI: 10.1063/5.0005078. eprint: https://doi.org/10.1063/5.0005078. URL: https://doi.org/10.1063/5.0005078.

[46] M. Zoppi et al. "Microscopic Structure and Intermolecular Potential in Liquid Deuterium". In: *Physical Review Letters* 75.9 (1995), pp. 1779–1782. DOI: 10.1103/physrevlett.75.1779. URL: https://app.dimensions.ai/details/publication/pub.1060811649.

[47] Daniele Colognesi et al. "Hydrogen self-dynamics in liquid $H_2 - D_2$ mixtures studied through inelastic neutron scattering". In: *Phys. Rev. E* 92 (1 July 2015), p. 012311. DOI: 10.1103/PhysRevE.92.012311. URL: https://link.aps.org/doi/10.1103/PhysRevE.92.012311.

[48] W. D. Seiffert, B. Weckermann, and R. Misenta. "Messung der Streuquerschnitte von flüssigem und festem Wasserstoff, Deuterium und Deuteriumhydrid für thermische Neutronen". In: *Zeitschrift für Naturforschung A* 25.6 (1970), pp. 967–972. DOI: 10.1515/zna-1970-0626. URL: https://app.dimensions.ai/details/publication/pub.1067569158.